AGRICULTURE AND NATURAL RESOURCES

Journal homepage: http://anres.kasetsart.org

Research article

Vision-based maize field zone classification for control of robot automatically dispensing granular fertilizer

Niramon Ruangpayoongsak*, Thanpisit Rangdeang, Chaithawat Puakhom

Production and Robotics Engineering Department, Faculty of Engineering, King Mongkut's University of Technology North Bangkok, Bangkok 10800, Thailand

Article Info

Article history:
Received 10 June 2025
Revised 5 September 2025
Accepted 3 October 2025
Available online 28 November 2025

Keywords:
Crop row navigation,
Fertilization,
State machine,
YOLO

Abstract

Importance of the work: Manual application of granular fertilizers is time-consuming and labor-intensive. Robot design and control are required to replace human labor.

Objectives: to develop and test an automatic granular fertilizer dispenser (AGFD) robot to replace human labor using a vision-based technique.

Materials and Methods: The problem of zone identification was investigated to locate the robot's position based on four defined zones: Front, Middle, Back and No-Row. A method was proposed to identify these maize field zones using the "You only look once" classification of red-green-blue (RGB) image frames obtained as the robot navigates in a maize field based on dead reckoning.

Results: The proposed method for zone identification, implementation of fertilizer system control and robot navigation in the maize field were successful. The fertilization and navigation control commands of the AGFD robot were successfully implemented with a success rate higher than 96% in real-time. The number of frames varied in the range 1,103–2,773 and the number of correct commands for each frame was counted. There was variation in the field conditions due to light, weeds, growth stages and shadows. When inconsistency occurred in the commands, the sequence of the designed state machine could prevent improper state changes and prevent unexpected behavior by the robot.

Main finding: The method of zone classification using front-view RGB images and the vision-based state machine design could successfully control the robot under various field conditions. The proposed zone classification could be applied to other types of robots and other row-crop types under field cultivation.

* Corresponding author.
E-mail address: niramon.r@eng.kmutnb.ac.th (N. Ruangpayoongsak)

https://doi.org/10.34044/j.anres.2025.59.6.05

Introduction

According YVP (2025), there are three stages of granular fertilization application. The first stage occurs when the crop is aged 0–20 d, the second stage occurs when the crop is aged 21–30 d and the third stage occurs when the crop is aged 31–45 d. Fig. 1 shows the manual application of granular fertilizer. Clearly, this method is time-consuming and labor-intensive.

A robot designed in 2016 to replace human labor is shown in Figs. 2A and 2B. The robot carries a granular fertilizer tank and has limit switches and wires to detect maize stems. The granular fertilizer is dropped every time a stem is detected on the left and right sides of the robot's body as the robot moves between the rows of the maize crop. The drawback of this method is the physical contact between the robot and the maize plant, which may damage the plant. Using physical contact is not the best way to control the fertilizing system.

Fig. 2A shows a computer-aided design schematic (Ruangpayoongsak and Kaewjan, 2017) and Fig. 2B shows a prototype of the fertilizing robot. The robot uses a differential drive driven by chains. The granular fertilizer dispenser is under the fertilizer tank. The fertilizing system consists of a cylindrical tank, direct current motors, valves and pipes. The valves control the dropping of granular fertilizer through the pipes on the left and right sides of the robot. The fertilizer dispenser releases fertilizer down the left and right sides of the robot to the maize stem via valves and pipes when the wire touches the maize stems and the limit switch sends a trigger signal. As shown in the block diagram of the AGFD robot in Fig. 2C, the Kinect V2 camera (HKConsole; Thailand) was mounted on the robot and connected to a Jetson Orin Nano Development Kit (Cytron; Thailand). The camera provides both high-resolution RGB images and depth information. The robot dimensions are 0.45 m × 0.75 m × 0.60 m, excluding the tank. The robot weights 22 kg, with an empty fertilizer tank and can carry 15 kg of granular fertilizer. Robot Operating System (ROS) is implemented for zone classification and robot control commands.

Fig. 1 Granular fertilizer being applied manually.

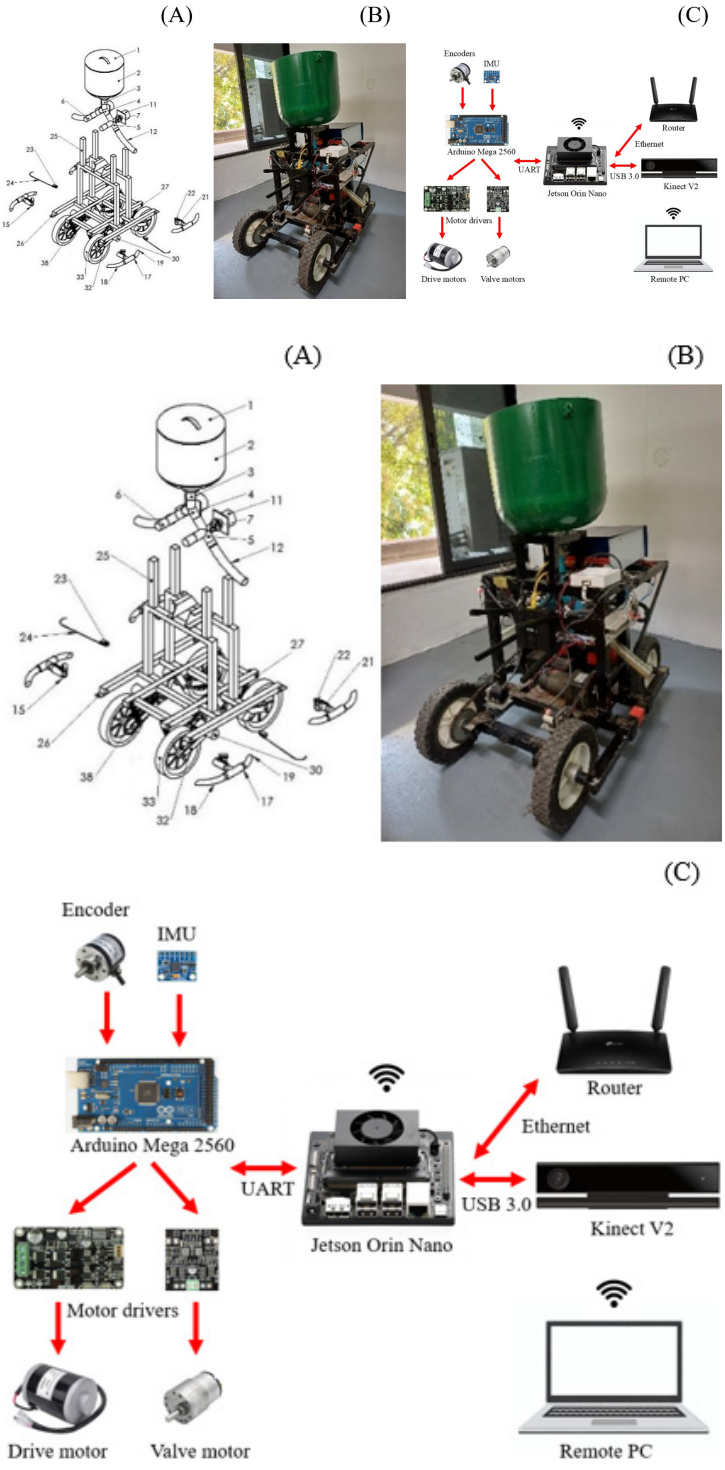

Fig. 2 Automatic granular fertilizer dispenser robot: (A) computer-aided design diagram (Ruangpayoongsak and Kaewjan, 2017); (B) prototype; (C) block diagram of process.

The current study developed a method that identified different zones in the maize field using the "you only look once" YOLO approach, requiring no physical contact between the robot and the maize, referred to as zone classification. The objectives were to propose a classification method and to generate control commands for fertilization and navigation of the AGFD robot. The contributions of the study were: the YOLO zone classification, the AGFD robot design and prototype and the state machines to control fertilization and navigation.

Recently, YOLO has been implemented for mobile robot navigation, with a method proposed to determine a navigation line for a corn-spraying robot based on an improved YOLOv8s network (Diao et al., 2023). The algorithm identified the corn plant core as the target and extracted the navigation line by fitting it using the least squares method. Yang et al. (2023) utilized YOLOv5 to detect crop rows by extracting a region of interest, computing feature points using the features from accelerated segment test to identify corner point and group them into crop rows based on fitting using the least squares method. Elsewhere, YOLOv5 was selected to identify crops and growth stages among maize and sugar beet (Cortinas et al., 2023).

In addition, YOLO has been applied to detect crops and weeds. Han et al. (2023) studied YOLOv4 with a crop detection model and the excess green index (ExG) to detect various weed species using top-view images. YOLOv5 with UAV images has been used to extract vegetation areas (Chen et al., 2024), in which the mean shift segmentation method combines the local variance segmentation evaluation function and the Otsu automatic classification method. Furthermore, Wang et al. (2024) developed YOLOv5 to detect weeds by incorporating a convolutional block attention module (CBAM), a FasterNet feature extraction network and a loss function to optimize the network structure.

YOLO has also been improved for different purposes in maize fields. Liu et al. (2024) applied an improved YOLOv4 to train a maize stem recognition model with an increased CBAM. Gao et al. (2022) developed YOLOv4 to combine with the channel pruning algorithm to detect the dropped ears of maize harvesters, where a k-means clustering algorithm was used to obtain a prior box matching the size of the dropped ears. Later, YOLOv5 was studied to detect maize leaf blight disease in complex scenarios (Leng et al., 2023), where the model extracts deep semantic information and fuses the feature map across maps at different scales. Recently, Li et al. (2024a) improved YOLOv8 to detect densely distributed maize leaf diseases.

Furthermore, various versions of YOLO have been used with top-view images acquired using UAVs. For example, UAV images were analyzed to detect the distribution characteristics of seedling emergence and growth using YOLOv3 (Liu et al., 2023). The performance by YOLOv3 was better than for YOLOv5 in detecting maize seedlings at various sites. A method was proposed to detect and count maize tassels based on UAV aerial images and YOLOv7 (Pu et al., 2023) and the density of maize in the field was assessed based on YOLOv7 (Wu et al., 2024). Ren et al. (2024) utilized YOLOv8 for an object detection algorithm with Voronoi spatial analysis to rapidly evaluate maize seedling quality based on high-resolution images taken using a UAV. YOLOv8 with a receptive field triplet attention convolution was proposed to detect and count the number of maize seedlings (Hao et al., 2024). YOLOv8 was selected to map maize planting densities (Shen et al., 2024). These methods are based on ultrahigh-definition imagery combined with object detection and multispectral remote sensing combined with machine learning.

Various vision-based techniques have been studied for crop row navigation. A machine vision approach was applied by Zheng et al. (2023) for early-stage maize crops to control an automatic row-oriented spraying system. Wei et al. (2024) recognized the crop row of maize at the seedling stage using a lightweight network. Guo et al. (2024a) detected crop row shapes using transformer-based parameter prediction and Li et al. (2024b) studied the segmentation and extraction of oilseed rape crop rows for visual navigation line extraction. An efficient Unet-based architecture for crop row segmentation was proposed by Guo et al. (2024b).

Various methods have been proposed to localize and navigate robots in crop fields. One research study detected the end of row using artificial landmarks (Vougioukas, 2019). Bergerman et al. (2015) and Ahmadi et al. (2020) developed navigation systems that used a two-dimensional (2D) laser scanner, with wheel and steering encoders. A monocular camera and odometer data were fused for localization to a reference map (Chebrolu et al., 2019). Fei and Vougioukas (2022) used a template of point clouds to detect the crop-row center line to navigate the robot. A crop-row detection algorithm was proposed for visual servoing in crop-row fields (De Silva et al., 2024). A finite state machine model for orchard navigation was proposed (Peng et al., 2023).

The current work differs from others (Peng et al., 2023; De Silva et al., 2024) in the following ways: 1) the Kinect V2 camera is mounted parallel to the ground with no tilting; 2) YOLO is selected to classify maize field zones based on detecting the features in each zone and classifying them into Front, Middle, Back and No-Row zones. The classified zones were defined as a finite state machine that controlled the fertilizing and navigation of the AGFD robot.

Materials and Methods

Zone definition: There were two aims in classifying the maize field zones: to control the fertilizing system and secondly to navigate in the field. The zones were classified into Front, Middle, Back and No-Row, as shown in Fig. 3. The Front zone is in the headland of the maize field when the robot faces the field before starting row navigation. The fertilizing system is turned off and the navigation is in Leading point mode. The Middle and Back zones are where the robot drives between rows in the maize crop, the fertilizing system is turned on and the navigation is in Inter-row navigation mode. The No-Row zone begins at the end of the row where the robot needs to turn to access the next row. The fertilizing system is turned off and the U-turn mode navigation begins.

Zone identification: Figs. 4A–4L show sample labelled images of the Front, Middle, Back and No-Row classes. The image data were collected under various field parameters, regarding lighting conditions, robot orientation, the size of the maize plant, background, weeds and shadows. The image data were collected from many maize fields in Kanchanaburi and Saraburi provinces, Thailand. The feature for identifying the Front zone was parts of the front of the maize field appearing in the image. In the Middle zone, the vanishing point and the rows appear. In the Back zone at the open end of the row, there is no vanishing point in the image. In the No-Row zone, there is no crop and only the background appears in an image.

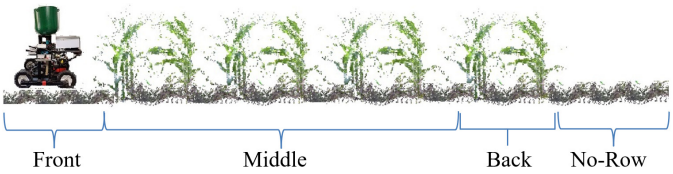

Fig. 3 Zone definition.

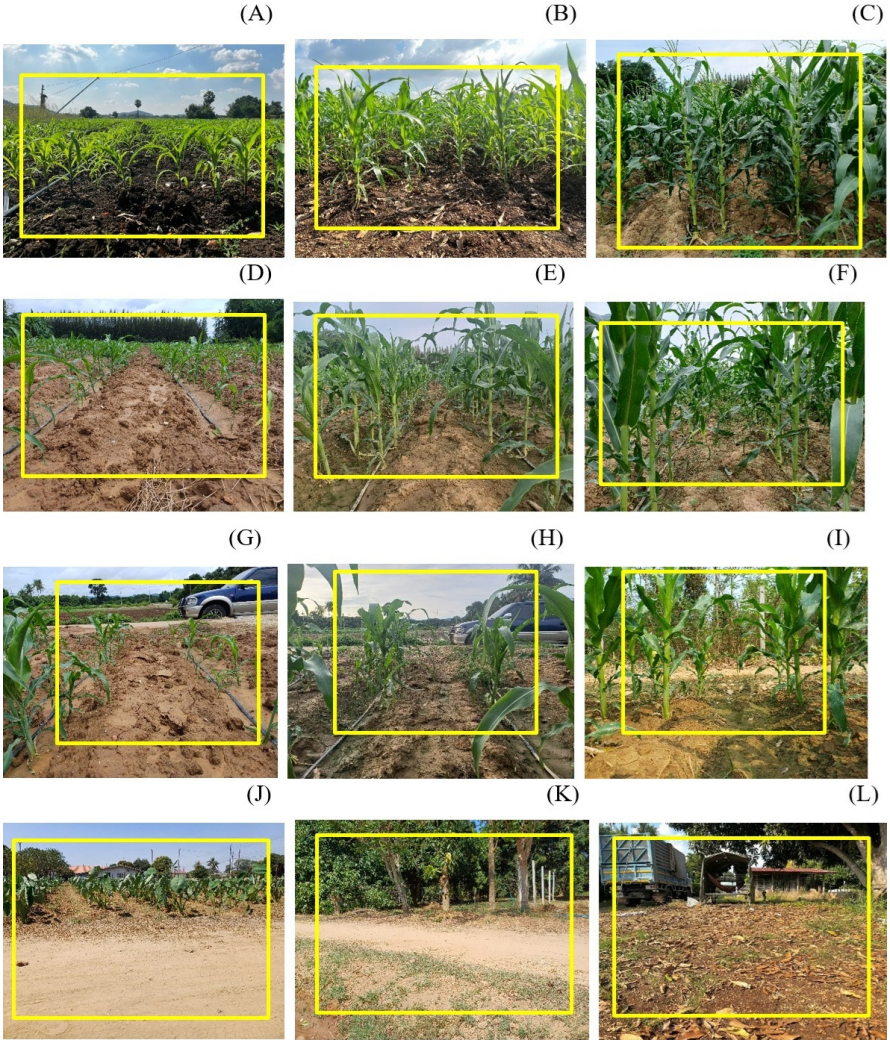

Fig. 4 images showing zones: (A–C) Front; (D–F) Middle; (G–I) Back; (J–L) No-Row, where yellow box indicates area of camera detection.

YOLO was selected for zone classification due to its high performance and success in agricultural applications (Gao et al. 2022 and Diao et al. 2023). Comparisons among versions was necessary to decide on the best version. The inference times on different platforms and versions are shown in Table 1. The training results for the YOLOv8n, YOLOv10n and YOLOv11n versions were all carried out using the same personal computer (PC), with each YOLO version being benchmarked with prior versions. Among the three evaluated models, YOLOv11n outperformed the others across most key performance indicators, producing the highest precision, recall and mean average precision (mAP) with a shorter training time than YOLOv8n. In addition, YOLOv11n produced the highest validation loss, indicating potential overfitting and reduced generalization. YOLOv8n, while slightly inferior in accuracy, maintained a low validation loss and demonstrated consistent performance. Figs. 5A and 5B show the confidence curve and normalized confusion matrix of YOLOv11n, where the number of epochs was 100. The model was trained using YOLO CLI (the Ultralytics command line interface; https://docs.ultralytics.com/usage/cli/) and the images were labeled using the image annotation tool LabelImg (https://pypi.org/project/labelImg/). The training-to-validation ratio in the dataset was 4:1, where the number of training images was 1042. YOLOv11n had the highest F1 value on the F1-confidence curve and represented all classes well, followed by YOLOv8n and YOLOv10n. The normalized confusion matrices indicated that the YOLOv11n validation result was superior to the other versions.

Fig. 6 shows the inference time of different YOLO versions on various platforms for an image size of 1920 pixels × 1080 pixels. The operating system was Ubuntu 20.04 (https://ubuntu.com/20-04). PyTorch (an open-source deep learning library; https://pytorch.org/) and CUDA (a proprietary parallel computing platform and application programming interface; https://developer.nvidia.com/cuda/toolkit) were installed on all platforms. The PC specifications were AMD Ryzen 2.30–4.0 GHz (https://www.amd.com/en/products/processors/desktops/ryzen.html), 16 GB RAM and a Nvidia GTX1650 GPU (https://www.nvidia.com/en-us/geforce/graphics-cards-1/gtx-1650/). The PC had the shortest inference time, followed by Jetson Orin Nano and Jetson Nano. YOLOv8n produced the shortest inference time, followed by YOLOv10n and YOLOv11n.

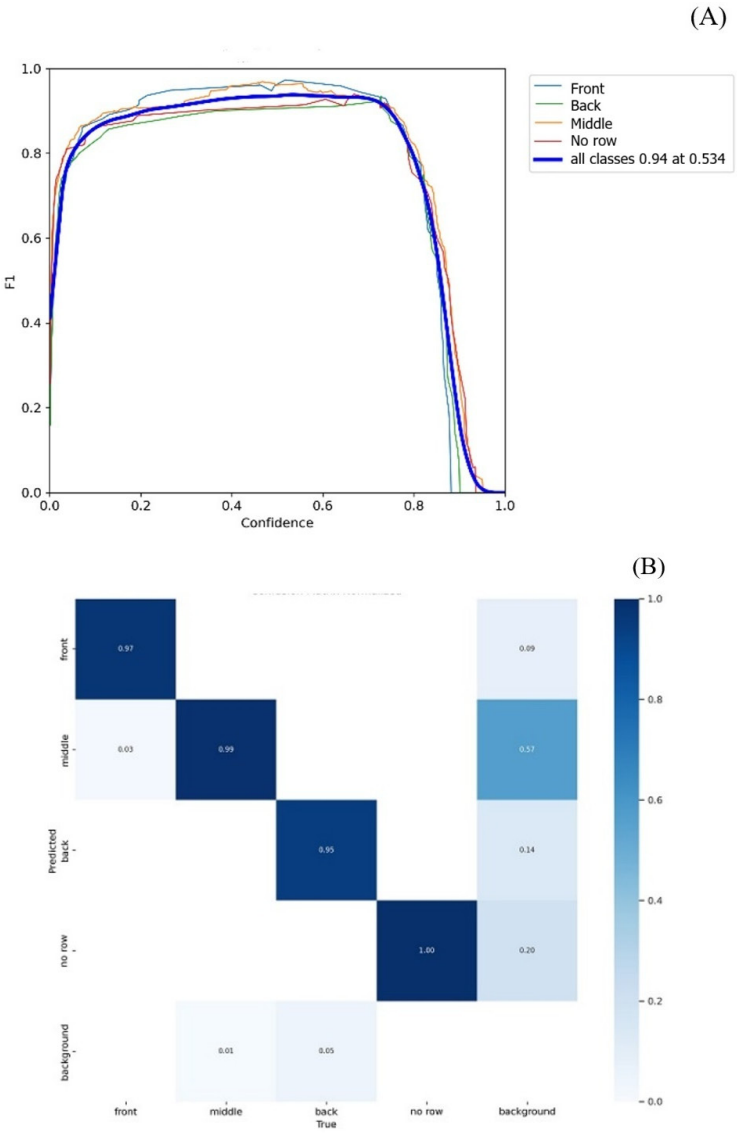

Fig. 5 Training output by zone based on YOLO v11n network: (A) confidence curve; (B) normalized confusion matrix.

Table 1 Training results for different "You only look once" (YOLO) versions.

Model	Training Time (s)	Precision	Recall	mAP50	mAP50-95
YOLOv8n	2061.97	0.8838	0.9447	0.94619	0.46647
YOLOv10n	1990.89	0.9014	0.8785	0.93864	0.49391
YOLOv11n	2003.56	0.9518	0.9521	0.96233	0.47544

mAP50 = Mean average precision at IOU over 0.5 ; mAP50-95 = Mean average precision at IOU over 0.5 to 0.95.

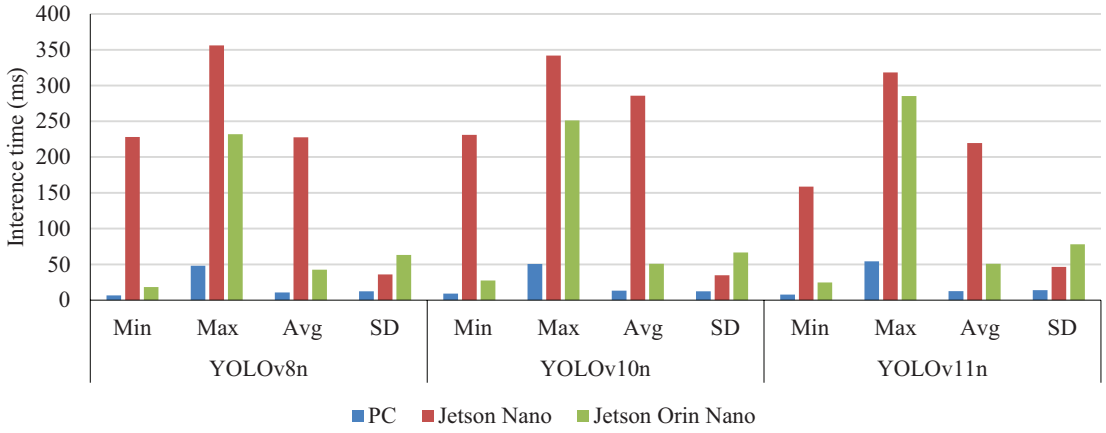

Fig. 6 Inference time on various platforms and "You only look once" (YOLO) versions, where Min = minimum, Max = maximum, Avg = average and PC = personal computer.

State machine: As shown in Fig. 7, the identified zones were used as a finite state machine. When the robot starts to operate, the Front should be the first zone found. Then, the robot moves forward into the Middle, Back and No-Row zones. When the robot makes a turn in the No-Row zone, it may detect the Front or Middle zone depending on the distance between the robot and the maize plant in front of it. If the robot is near the crop, it may find the Middle instead of the Front zone. After that, the next zones would be Back and No-Row, respectively. As the robot never moves backward, the sequence will always be a loop containing Front, Middle, Back, No-Row, Front/Middle, Back and No-Row.

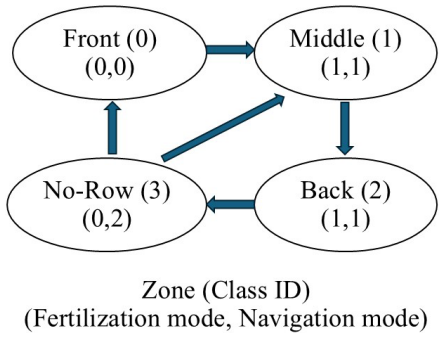

Fig. 7 Different machine states in different zones for fertilization and navigation modes.

Two fertilization modes were tested: 0 (Off) and 1 (On), with the fertilizing system of the robot being controlled by turning the tank valve on or off. When the valve is open, the fertilizer falls through the pipe and drops onto the stem of the maize plant on both the left and right rows simultaneously. The control signal is sent from Arduino command-line interface (https://docs.arduino.cc/arduino-cli/) to the tank valve. In the Middle and Back zones, the valve is turned on, whereas in the Front and No-Row zones, the valve is turned off. The valve control command must be checked regularly for consistency in the same zone to allow the fertilizer to drop continuously.

Navigation is divided into three modes: Leading Point (0), Inter-Row (1) and U-turn (2). The Leading Point Search (Suriyakoon and Ruangpayoongsak, 2017) determines the robot's heading direction during Leading Point navigation in the Front zone. The inter-row navigation mode is used when the robot is in the Middle and Back zones, whereas the robot's heading is controlled to stay on the center line between rows. Later, when the robot enters the No-Row zone, the navigation mode is changed to U-turn navigation. In this mode, the robot turns to the next row.

Evaluation indices: Based on YOLO evaluation indices (Diao et al., 2023), the precision (P), recall (R), $F1$ score and mean average precision (mAP) were defined using Eq. (1)–Eq. (4):

$$P = \frac{T_p}{T_p + F_p} \times 100\% \quad (1)$$

$$R = \frac{T_p}{T_p + F_N} \times 100\% \quad (2)$$

$$F1 = \frac{2PR}{P+R} \times 100\% \quad (3)$$

$$mAP = \frac{1}{n}\sum_{i=1}^{n} AP_i, AP = \int_0^1 P(R)dR \quad (4)$$

where T_p is the true positive, F_p is the false positive, and F_n is the false negative.

Results and Discussion

Fig. 8 shows the AGFD robot in a maize field during data collection and field testing. YOLOv11n was implemented on a Jetson Orin Nano Development Kit (Cytron; Thailand). This section presents the training results of YOLOv11n, including inference samples and real-time inference results.

Normalized confusion matrix: YOLOv11n was selected for deployment in the fertilization robot system due to its superior balance between detection accuracy and model stability, which are critical for real-time agricultural field operations. Fig. 9 shows the precision-recall curve of YOLOv11n, which is a good classifier.

Inferencing results: Figs. 10A–10D show a frame of the YOLO inferencing results for Front, Middle, Back and No-Row zones. Analysis is based on detection within the boundary box in the result images with the predicted zone and confidence value in the top-left corner. The yellow boxes in the images show the labelling in the dataset. As the robot moves forward, the detection box appears continuously with varied box sizes, zones and confidence values.

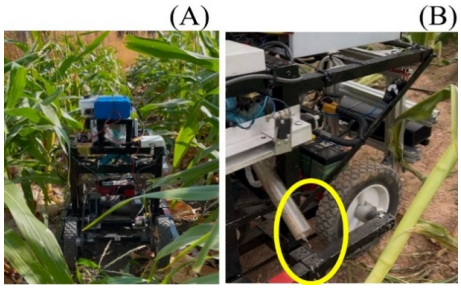

Fig. 8 Automatic granular fertilizer dispenser robot: (A) data collection and field test; (B) dropping granular fertilizer (yellow circle).

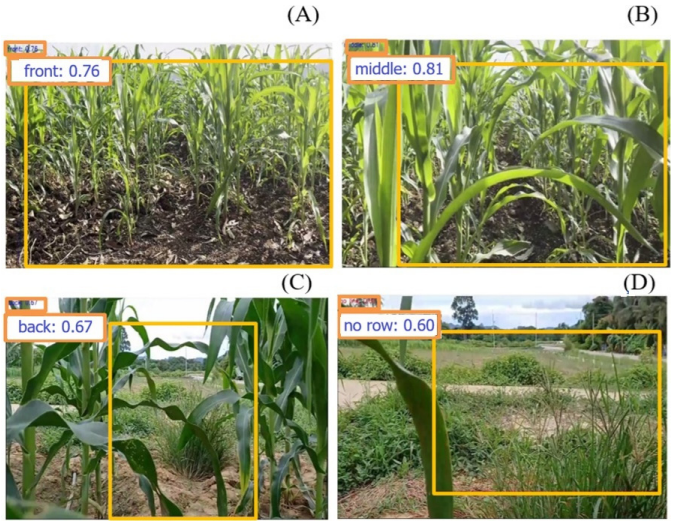

Fig. 10 Inferencing results by zone based on YOLO v11n network: (A) Front; (B) Middle; (C) Back; (D) No-Row.

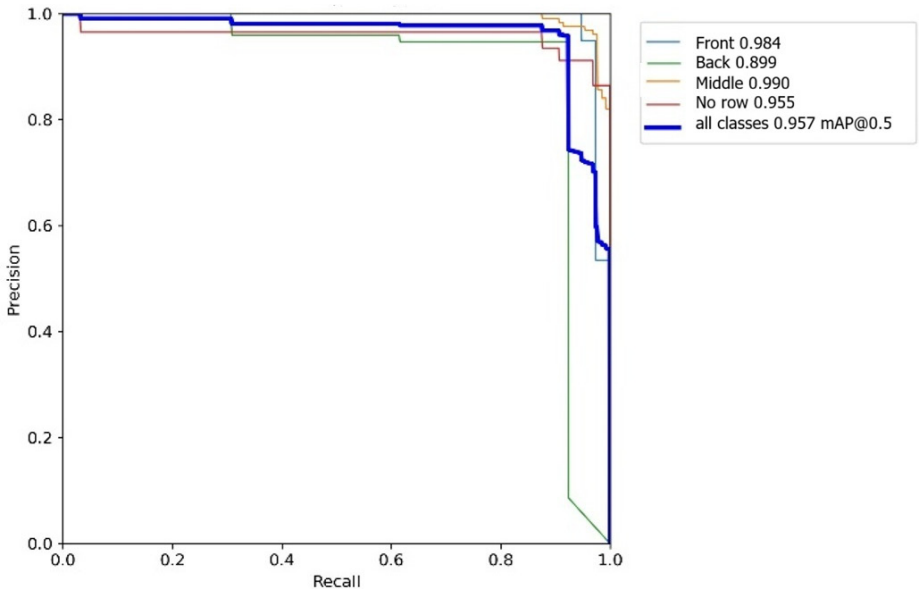

Fig. 9 Precision-recall curve based on YOLO v11n network.

Real-Time Testing: In the field test, the robot was teleoperated. To verify the continuity and correctness of fertilizing and navigation commands in real-time, the prediction of zone classification by YOLOv11n is presented in this section. The maize field conditions were: lighting condition (high, medium, low); presence of weeds (none, light, medium, dense); growth stage (small, medium, large); and presence of shadows (none, present). Fig. 11 shows the zone, fertilization mode and navigation mode of the image sequences.

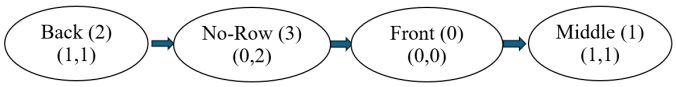

Fig. 11 Sequence of zones in testing.

Fig. 12 shows a sample of the results. The class ID (Zone), the fertilizing mode (F) and the navigation mode (N) of each frame were plotted. In each trial, the robot started in the Middle (1) zone, proceeded into the Back (2) zone, entered the No-Row (3) zone and turned to the next row in the Front (0) or Middle (1) zones, respectively. The fertilizing system was turned on (1) at the beginning and later was turned off (0) or on (1), corresponding to the classified zone, whereas the navigation mode was switched from Inter-row navigation (1) to U-turn (2) and Leading point (0) and back to Inter-row navigation (1). Between frame numbers 479–497, 811–830, 1088–1027 and 1853–1863, the classified zone switched between zones. Therefore, the fertilizing system was switched on and off during this period and the navigation mode switched between modes.

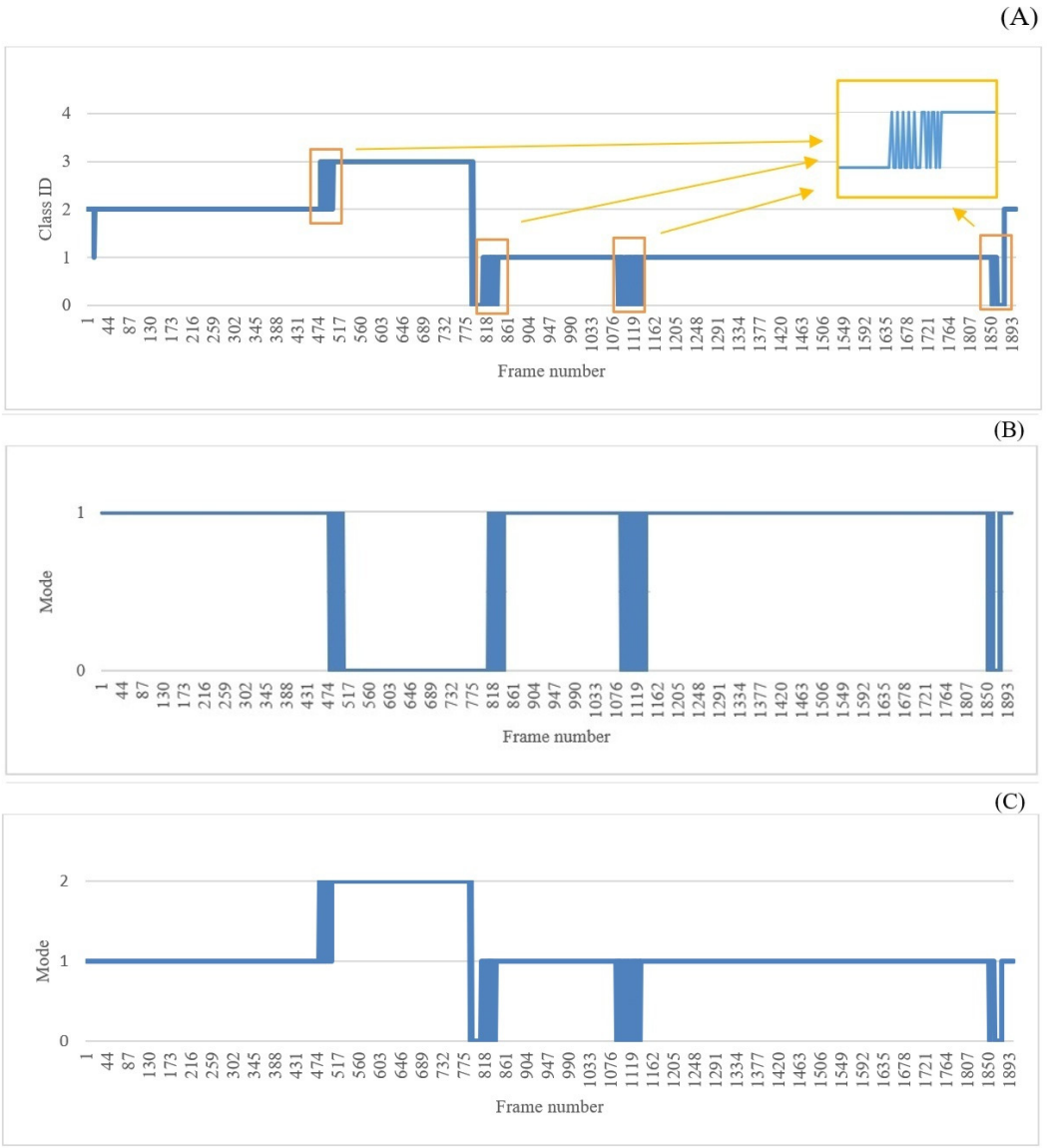

Fig. 12 Output from YOLO inferencing and generated control commands: (A) zone classification; (B) control commands for fertilization; (C) control commands for navigation.

However, the commands were inconsistent. To solve this, filtering for the zone classification was required to prevent unexpected robot behavior. The filter prevented a zone reversal. For example, if the zone No-Row were detected for more than five frames, the zone would be changed permanently to No-Row and not revert to Back.

Table 2 lists the field conditions of each trial differentiated by lighting condition, weed condition, growth stage and the presence of shadows. Table 3 shows the number of correct fertilization and navigation commands without filtering the classified zone. The average correctness of the fertilization control command was 96.19% and for the navigation command was 96.27%. As expected, the zone could be identified in various field conditions using YOLO. Low correctness was recorded in trials 5 and 10, where the growth stage was small. High correctness was recorded in trials 2 and 9, where the growth stage was medium and large.

Fig. 13 shows a screenshot of real-time testing. The system, encapsulating an ROS node, processed RGB images captured from the /kinect2/qhd/image_color_rect/compressed topic. The fertilizing status is displayed on the screen.

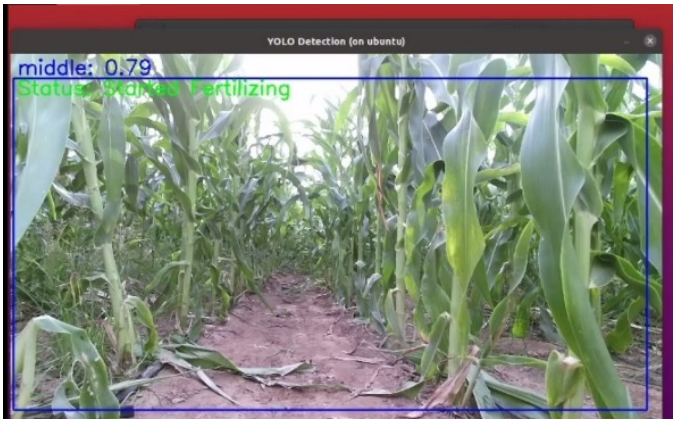

Fig. 13 Screenshot from ROS of real-time testing. The "Middle" zone is detected and the fertilizing status is started.

The current results differed from others in that the outputs are determined for the fertilizing system, which can be applied to other similar robots. Furthermore, the current study applied three navigation modes, whereas other works reported only two modes (the Leading Point mode was not presented in other works). Notably, the Leading Point mode helps to increase the functionality of the heading control after a U-turn and before entering the next row.

Table 2 Field conditions for each trial.

Trial number	Light condition	Weed condition	Growth stage	Presence of shadows
1	High	None	Small	None
2	High	None	Medium	Present
3	High	Medium	Small	Present
4	High	Medium	Medium	Present
5	High	Dense	Small	Present
6	High	Dense	Large	Present
7	Medium	Sparse	Medium	None
8	Medium	Sparse	Large	None
9	Medium	Medium	Large	None
10	Low	None	Small	None
11	Low	Medium	Medium	Present

Table 3 Correctness of control fertilization and navigation commands.

Trial number	Number of frames	Number of correct fertilization commands		Number of correct navigation commands	
		(frames)	(%)	(frames)	(%)
1	1,159	1,120	96.63	1,120	96.63
2	2,773	2,749	99.13	2,749	99.13
3	1,755	1,727	98.40	1,727	98.40
4	2,373	2,326	98.02	2,326	98.02
5	1,249	1,132	90.63	1,132	90.63
6	1,661	1,631	98.19	1,631	98.19
7	2,271	2,124	93.52	2,123	93.48
8	2,240	2,187	97.63	2,187	97.63
9	2,518	2,493	99.00	2,493	99.00
10	1,103	998	90.40	1,101	91.58
11	1,903	1,838	96.58	1,833	96.32
			96.19		96.27

There were several advantages of the current method compared to vision-based crop row navigation (De Silva et al., 2024): In the current work, the camera is front-facing and the field of view (FOV) of the camera can cover various sizes of maize, whereas the other work used a tilting camera, whose FOV could cover only small maize sizes, which was not suitable for implementation on the AGFD robot to fertilize the three stages of maize. In addition, the current approach use four states (Front, Middle, Back, No-Row) in the state machine instead of three states (A, B, C), since the current approach defined differences in state A as Front and Middle to control the robot in the Front state, which was not considered in the other work. Furthermore, the current approach improved the state machine by adding the Front state, so when the robot turned into the next row—into the Front state instead of the Middle (state A) state—the robot could continue in Leading point mode without getting stuck.

A orchard navigation study (Peng et al., 2023) used four states (START, END, IN_ROW_Navigate and U_TURN_Navigate) and utilized a 3D point cloud to determine the state instead of the image data. However, a limitation of this approach is that the headland width must be longer than 5 m. In contrast, the current method applies a vision-based technique that unlike the point cloud-based technique has no limitation on the size of the headland.

In conclusion, the current study considered the zone identification problem, zone classification using YOLO, the AGFD robot and control of fertilization and navigation. Different versions of YOLO were compared and YOLOv11n was selected for robot control due to its superior performance compared to the other tested YOLO versions. The experimental results from the YOLO classification and inference indicated the YOLO model training was successful. In addition, the trained model was tested in various maize fields under different conditions to verify its performance. The average correctness of fertilization control command was 96.19% and for navigation command was 96.27%. Thus, the proposed zone identification method could control fertilization and navigation in real-time. The proposed method could be applied to other low-cost RGB cameras and would help to reduce the cost of crop row robots in precision agriculture. The fertilizing command could be applied to spraying, weeding, monitoring or other types of robotic operation in other types of row-crop field cultivation.

Conflict of Interest

The authors declare that there are no conflicts of interest.

References

Ahmadi, A., Nardi, L., Chebrolu, N., Stachniss, C. 2020. Visual servoing-based navigation for monitoring row-crop fields. In: Proc. 2020 IEEE International Conference on Robotics and Automation (ICRA), Paris, France, pp. 4920–4926.

Bergerman, M., Maeta, S.M., Zhang, J., Freitas, G.M., Hamner, B., Singh, S., Kantor, G. 2015. Robot farmers: Autonomous orchard vehicles help tree fruit production. IEEE Robot. Autom. Mag. 22: 54–63. doi.org/10.1109/MRA.2014.2369292

Chebrolu, N., Lottes, P., Läbe, T., Stachniss, C. 2019. Robot localization based on aerial images for precision agriculture tasks in crop fields. In: Proc. 2019 IEEE International Conference on Robotics and Automation (ICRA). Montreal, QC, Canada, pp. 1787–1793.

Chen, P., Xia, T., Yang, G. 2024. A new strategy for weed detection in maize fields. Eur. J. Agron. 159: 127289. doi.org/10.1016/j.eja.2024.127289

Cortinas, E., Emmi, L., Gonzalez-de-Santos, P. 2023. Crop identification and growth stage determination for autonomous navigation of agricultural robots. Agronomy 13: 2873. doi.org/10.3390/agronomy13122873

De Silva, R., Cielniak, G., Gao, J. 2024. Vision-based crop row navigation under varying field conditions in arable fields. Comput. Electron. Agric. 217: 108581. doi.org/10.1016/j.compag.2023.108581

Diao, Z., Guo, P., Zhang, B., et al. 2023. Navigation line extraction algorithm for corn spraying robot based on improved YOLOv8s network. Comput. Electron. Agric. 212: 108049. doi.org/10.1016/j.compag.2023.108049

Fei, Z., Vougioukas, S. 2022. Row-sensing templates: A generic 3D sensor-based approach to robot localization with respect to orchard row centerlines. J. Field Robot. 39: 712–738. doi.org/10.48550/arXiv.2107.01321

Gao, A., Geng, A., Zhang, Z., Zhang, J., Hu, X., Li, K. 2022. Dynamic detection method for falling ears of maize harvester based on improved YOLO-V4. Int. J. Agric. Biol. Eng. 15: 22–32. doi.org/10.25165/j.ijabe.20221503.6660

Guo, Z., Geng, Y., Wang, C., et al. 2024b. InstaCropNet: An efficient Unet-based architecture for precise crop row detection in agricultural applications. Artif. Intell. Agric. 12: 85–96. doi.org/10.1016/j.aiia.2024.05.002

Guo, Z., Quan, L., Sun, D., et al. 2024a. Efficient crop row detection using transformer-based parameter prediction. Biosyst. Eng. 246: 13–25. doi.org/10.1016/j.biosystemseng.2024.07.016

Han, X., Wang, H., Yuan, T., et al. 2023. A rapid segmentation method for weed based on CDM and ExG index. Crop Prot. 172: 106321. doi.org/10.1016/j.cropro.2023.106321

Hao, F., Zhu, S., Ma, D., Dong, X., Kong, H., Liu, X., Mu, C., 2024. Rapid maize seedling detection based on receptive-field and cross-dimensional information interaction. In: Proc. IEEE Int. Conf. Systems, Man and Cybernetics, pp. 2120–2125.

Leng, S., Musha, Y., Yang, Y., Feng, G. 2023. CEMLB-YOLO: Efficient detection model of maize leaf blight in complex field environments. Appl. Sci. (Switz.) 13: 9285. doi.org/10.3390/app13169285

Li, G., Le, F., Si, S., Cui, L., Xue, X. 2024b. Image segmentation-based oilseed rape row detection for in-field navigation of agri-robot. Agronomy 14: 1886. doi.org/10.3390/agronomy14091886

Li, R., Li, Y., Qin, W., et al. 2024a. Lightweight network for corn leaf disease identification based on improved YOLOv8s. Agriculture (Switz.) 14: 220. doi.org/10.3390/agriculture14020220

Liu, M., Su, W.H., Wang, X.Q. 2023. Quantitative evaluation of maize emergence using UAV imagery and deep learning. Remote Sens. (Basel) 15: 1979. doi.org/10.3390/rs15081979

Liu, M., Zhang, X., Wang, X., Wei, Z., Cheng, X. 2024. Research on maize stem recognition based on machine vision. Eng. Agric. 44: 2024. doi.org/10.1590/1809-4430-ENG.AGRIC.V44E20240028/2024

Peng, C., Fei, Z., Vougioukas, S.G. 2023. GNSS-free end-of-row detection and headland maneuvering for orchard navigation using a depth camera. Machines 11: 84. doi.org/10.3390/machines11010084

Pu, H., Chen, X., Yang, Y., Tang, R., Luo, J., Wang, Y., Mu, J. 2023. Tassel-YOLO: A new high-precision and real-time method for maize tassel detection and counting based on UAV aerial images. Drones 7: 492. doi.org/10.3390/drones7080492

Ren, L., Li, C., Yang, G., et al. 2024. Detection of maize seedling quality from UAV images based on deep learning and Voronoi diagram algorithms. Remote Sens. (Basel) 16: 3548. doi.org/10.3390/rs16193548

Ruangpayoongsak, N., Kaewjan, T. 2017. Granule fertilizing dispenser robot in maize field. Thailand Petty Patent 12263, 5 Jan 2017.

Shen, J., Wang, Q., Zhao, M., et al. 2024. Mapping maize planting densities using unmanned aerial vehicles, multispectral remote sensing and deep learning technology. Drones 8: 140. doi.org/10.3390/drones8040140

Suriyakoon, S., Ruangpayoongsak, N. 2017. Leading point-based interrow robot guidance in corn fields. In: Proc. 2017 2nd International Conference on Control and Robotics Engineering (ICCRE), Bangkok, Thailand, 1–3 Apr 2017; pp. 8–12.

Vougioukas, S.G. 2019. Agricultural robotics. Annu. Rev. Control Robot. Auton. Syst. 2: 365–392. doi.org/10.1146/annurev-control-053018-023617

Wang, X., Wang, Q., Qiao, Y., Zhang, X., Lu, C., Wang, C. 2024. Precision weed management for straw-mulched maize field: Advanced weed detection and targeted spraying based on enhanced YOLOv5s. Agriculture (Switz.) 14: 2134. doi.org/10.3390/agriculture 14122134

Wei, J., Zhang, M., Wu, C., Ma, Q., Wang, W., Wan, C. 2024. Accurate crop row recognition of maize at the seedling stage using lightweight network. Int. J. Agric. Biol. Eng. 17: 189–198. doi.org/10.25165/j.ijabe.20241701.7051

Wu, W., Zhang, J., Zhou, G., Zhang, Y., Wang, J., Hu, L. 2024. ESG-YOLO: A method for detecting male tassels and assessing density of maize in the field. Agronomy 14: 241. doi.org/10.3390/agronomy 14020241

Yang, Y., Zhou, Y., Yue, X., Zhang, G., Wen, X., Ma, B., Xu, L., Chen, L. 2023. Real-time detection of crop rows in maize fields based on autonomous extraction of ROI. Expert Syst. Appl. 213: 118826. doi.org/10.1016/j.eswa.2022.118826

YVP. 2025. Maize fertilization. https://yvpgroup.com/corn-fertilizer/, 10 March 2025.

Zheng, K., Zhao, X., Han, C., He, Y., Zhai, C., Zhao, C. 2023. Design and experiment of an automatic row-oriented spraying system based on machine vision for early-stage maize crops. Agriculture 13: 691. doi.org/10.3390/agriculture13030691